MASTER

COO-3158-50

# A COMPUTER-CONTROLLED TIME-OF-FLIGHT ATOM-PROBE FIELD-ION MICROSCOPE FOR THE STUDY OF DEFECTS IN METALS

Thomas M. Hall,† Alfred Wagner and David N. Seidman

Cornell University
Ithaca, New York 14853

August 1976

NOTICE
This report was prepared as an account of work sponsored by the United States Government. Neither the United States nor the United States Energy Research and Development Administration, nor any of their employees, nor any of their contractors, subcontractors, or their employees, makes any warranty, express or implied, or assumes any legal liability or responsibility for the accuracy, completeness or usefulness of any information, apparatus, product or process disclosed, or represents that its use would not infringe privately owned rights.

Prepared for
THE U.S. ENERGY RESEARCH AND DEVELOPMENT ADMINISTRATION
UNDER CONTRACT NO. EY-76-S-02-3158.*000

Report #2693
Issued by
The Materials Science Center

† Now at Bell Laboratories, 555 Union Boulevard, Allentown, Pennsylvania 18103

DISTRIBUTION OF THIS DOCUMENT IS UNLIMITED

## DISCLAIMER

This report was prepared as an account of work sponsored by an agency of the United States Government. Neither the United States Government nor any agency Thereof, nor any of their employees, makes any warranty, express or implied, or assumes any legal liability or responsibility for the accuracy, completeness, or usefulness of any information, apparatus, product, or process disclosed, or represents that its use would not infringe privately owned rights. Reference herein to any specific commercial product, process, or service by trade name, trademark, manufacturer, or otherwise does not necessarily constitute or imply its endorsement, recommendation, or favoring by the United States Government or any agency thereof. The views and opinions of authors expressed herein do not necessarily state or reflect those of the United States Government or any agency thereof.

**DISCLAIMER**

**Portions of this document may be illegible in electronic image products. Images are produced from the best available original document.**

# A COMPUTER-CONTROLLED TIME-OF-FLIGHT ATOM-PROBE FIELD-ION MICROSCOPE FOR THE STUDY OF DEFECTS IN METALS*

by

Thomas M. Hall,† Alfred Wagner and David N. Seidman

Cornell University, Bard Hall,
Department of Materials Science and Engineering and the
Materials Science Center, Ithaca, New York 14853

## ABSTRACT

A time-of-flight (TOF) atom-probe field-ion microscope (FIM) specifically designed for the study of defects in metals is described. This atom probe features: (1) a variable magnification internal-image-intensification system based on a channel electron multiplier array (CEMA) for viewing the FIM image; (2) a liquid-helium-cooled goniometer stage which allows the specimen to be maintained at a temperature anywhere in the range of 13 to 450 K; (3) a low energy ($\leq$3 keV) gas ion gun for in-situ irradiations; (4) an ultra-high vacuum ($\sim 3 \cdot 10^{-10}$ Torr) chamber to minimize specimen contamination; (5) a high-vacuum ($\sim 10^{-6}$ Torr) specimen-exchange device; (6) a Chevron ion detector; and (7) an eight-channel digital timer with ± 10 nsec resolution for measuring the TOFs of the pulse-field evaporated ions. The entire process of applying the evaporation pulse to the specimen, measuring the dc and pulse voltages, and analyzing the TOF data is controlled by a Nova 1220 computer. Data in the form of a histogram of the number of events versus the mass-to-charge ratio is displayed on a Tektronix graphics terminal. An extensive set of computer programs to test and operate the atom-probe FIM have also been developed. With this automated system we can presently record and analyze 600 TOF $min^{-1}$. The instrument can clearly resolve the seven isotopes of molybdenum and the five isotopes of tungsten. Investigations of alloys have shown that the concentration of rhenium in a W-25 at.% Re alloy; and the concentrations of titanium and zirconium in a Mo-1.0 at.% Ti alloy and a Mo-1.0 at.% Ti - 0.08 at.% Zr alloy can be easily measured. Investigations of a low swelling stainless steel alloy (LS1A) and a metallic glass alloy (Metglas 2826) have shown that all constituents present at a level of 0.05 at.% or higher can be readily determined.

---

* Research supported by the Energy Research and Development Administration. Additional support was received from the National Science Foundation through the use of the technical facilities of the Materials Science Center at Cornell University.

† Now at Bell Laboratories, 555 Union Boulevard, Allentown, Pennsylvania 18103

## 1. Introduction

The time-of-flight (TOF) atom-probe field-ion microscope (FIM)† is basically a FIM combined with a special TOF mass spectrometer (Müller, Panitz and McLane 1968). Figure 1 illustrates the main features of the atom probe. A specimen with a radius of ∿50 to 500 A is maintained at a positive potential of ∿5 to 20 kV so that gas atoms surrounding the specimen are ionized over individual atomic sites and are projected radially outward to produce an image of the atoms on the internal-image-intensification system. When a short high-voltage pulse is applied atoms on the surface of the specimen are field evaporated in the form of ions. Those ions projected into the probe hole at the center of the internal-image-intensification system will pass down the flight tube to the Chevron ion detector. The TOFs of the ions and the voltage on the specimen are measured and used to determine the mass-to-charge ratios (m/n) of the field-evaporated ions. The operation of the atom probe is controlled on line by a Nova 1220 minicomputer which triggers the high voltage pulse to the tip, reads in the TOF and voltage data, and then calculates the (m/n) values of the ions. The computer operates in real time so that results are available immediately on the graphics display terminal for interpretation as the experiment progresses.

† The TOF atom-probe FIM will simply be referred to as an atom probe in this paper.

Since the first publication concerning an atom probe by Müller, Panitz and McLane (1968) a number of other instruments have also been reported in the literature and also described at Field Emission Symposia (Brenner and McKinney 1968, Brenner and McKinney 1970, Turner, Regan and Southon 1973, Kinosita, Nakamura and Kuroda 1974, Wagner, Hall and Seidman 1975, Gallot, Sarru and Bostel 1975, Lewis and Smith 1975, Watts and Ralph 1975, Chambers and Ehrlich 1975, Andren and Norden 1975, Krautz, Ladurner and Leisch 1976). The major metallurgical applications of the atom probe to date are as follows: (1) a study of the early stages of precipitation in Fe(Cu) alloys by Goodman, Brenner and Low (1973a and 1973b) and in the Fe-3at.% Mo system (Brenner and Goodman 1971); (2) the analysis of precipitates in iron and steels by Turner and Papazian (1973); and (3) an investigation of chromium depletion near the surface of a 410 stainless steel by Krishnaswamy, McLane and Müller (1974). In addition, Müller and Tsong (1973) and Panitz (1975) have written extensive review articles on the subject of single atom mass spectrometry to which the reader is referred for further details on the physics of the atom probe.

The atom probe is ideally suited for the study of the interactions of lattice

defects with impurity atoms and alloying elements in metals. The basic reason for this fact is that by controlled pulse-field evaporation of successive atomic layers it is possible to examine the bulk of the specimen and to reconstruct in three dimensions the correspondence between specific microstructural features and chemical composition. More specifically the atom probe is capable of imaging lattice defects such as vacancies, self-interstitial atoms (SIAs), dislocations, grain boundaries, and voids and can also chemically identify both substitutional and interstitial alloying elements or impurity atoms.

In Sections 2 through 4 of this paper we describe an ultra-high-vacuum (UHV), computer controlled atom probe with a number of unique features that make it ideally suited for studying metallurgical problems and in particular for the study of defects in metals. Many details concerning the actual construction of this instrument are contained in an unpublished report (Hall et al. 1975) which has been briefly summarized in a short paper (Hall et al. 1976). Section 5 of this article contains the results of a number of atom probe experiments which demonstrate the instrument's ability to examine a wide variety of pure metals, metal alloys, and metallic glasses.

## 2. Field-ion microscope system

### 2.1. Internal image-intensification system and focusing lens

As shown in figure 1 the FIM image is observed with the aid of an internal image-intensification system consisting of a Galileo 75mm diameter channel-electron-multiplier array (CEMA) and a phosphor screen (Rosebury 1965). The CEMA has a particle gain of $>10^3$ which makes direct observation of the FIM image easy even at an imaging gas pressure as low as $10^{-6}$ Torr[†] (Turner et al. 1969, Brenner and McKinney 1970). The beam of pulse-field evaporated ions, which pass through the 3mm hole in the internal image-intensification system, is shielded from the potentials on the CEMA and screen by a 25 μm thick wall stainless steel tube at ground potential. This tube is electrically insulated from the CEMA and screen by a 50 μm thick wall glass tube. To further shield the ion beam, the back side of the glass screen was given a separate coating of tin oxide which is also maintained at ground potential.

[†] All pressures reported in this text are gauge pressures.

Immediately behind the image intensification system (see figure 1) is a focusing lens in the form of a stainless steel bushing which passes through a glass plate coated on both sides with tin oxide. This lens is maintained at a voltage which is proportional to the dc voltage on the specimen (see Section 3.1).

Behind the focusing lens is a front-surfaced glass mirror, placed at an angle of 45° with respect to the flight path, which contains a 10mm diameter hole through its center. The hole through the mirror is lined with a grounded stainless steel metal sleeve which prevents charged particles from accumulating on the exposed glass surfaces. The FIM image is photographed with an Automax 35 mm ciné camera.

The entire assembly consisting of the internal image intensification system, focusing lens, and viewing mirror is attached to two UHV metal bellows (Metal Bellows Co., Sharon, MA) arranged so that the distance from the tip of the specimen to the front surface of the image intensification system is continuously variable. By this means the tip-to-image intensification system distance can be varied from ∿12 to 100mm thus providing a lineal magnification change of ≳8x and an areal magnification change of ≳64x.

2.2. Helium-cooled goniometer stage

A liquid helium-cooled goniometer stage has been constructed which has the following features: (1) the specimen can be quickly cooled to cryogenic temperatures to improve the quality and resolution of the FIM image and also to change the diffusivity of point defects such as SIAs; (2) the specimen can be rotated by ± 35 degrees, about two orthogonal axes which intersect at the tip of the specimen so that a selected region of the specimen can be projected over the probe hole for chemical analysis; and (3) the goniometer stage can be translated in three mutually orthogonal directions (x, y, and z) to facilitate the alignment of the tip with respect to both the probe hole and the low-energy gas ion-gun described in Section 2.3.

A cutaway view of the helium-cooled goniometer stage is shown in figure 2. The FIM specimen is mounted in a copper specimen holder that is removed when one specimen is exchanged for another. This copper specimen holder is threaded into a copper plate which is bolted onto the back of the upper sapphire electrical insulator. On the top of this sapphire insulator is a copper plate into which are clamped 25 strands of 0.3mm diameter high purity gold wire. The upper end of this inner cooling braid is clamped to the lower end of the cryostat. The liquid helium cryostat is similar to the one described previously by Seidman et al. (1969), but the design has been modified to take increased advantage of the cooling power of the cold helium gas produced by the liquid helium that boils off during the initial cooldown period.

The conduction heat load on the specimen holder was minimized by supporting the sapphire block containing the specimen holder on a 50 μm thick wall stainless steel tube. The radiation heat load was minimized by surrounding the specimen holder with a copper radiation shield that is cooled to within 50 K of the tip

temperature by the helium exhaust gas escaping from the cryostat. Because of these features the total heat load on the specimen holder is small (∿0.3W) compared to the total cooling capacity of the gold braid (∿5W). Tests of the cryostat's performance showed that the FIM specimen is cooled to 30 K within ∿20 min and to 13 K within 1 hour with a liquid helium consumption rate of ∿1.5ℓhr$^{-1}$ at 13 K. At temperatures greater than ∿30 K the consumption rate drops to ∿0.1ℓhr$^{-1}$. In routine operation the temperature is measured with a platinum resistance thermometer (PRT) located on the tail of the liquid helium cryostat (see figure 2). The specimen temperature has been calibrated with respect to this PRT.

The goniometer supporting the cryostat was adapted from plans generously supplied by Dr. S. S. Brenner of the U. S. Steel Corporation. This goniometer provides the rotation about two orthogonal axes while maintaining UHV conditions by the use of two linear-motion stainless steel UHV bellows seals. Due primarily to the compact design of the goniometer stage the lateral position of the tip varies by less than 1mm when the tip is rotated through its full arc. The portion of the goniometer external to the FIM is mounted on three machinist's slides and is connected to the vacuum system through a bellows seal so that it can be translated in three mutually orthogonal directions to facilitate alignment of the tip with respect to the flight tube and the ion gun.

2.3. Low-energy gas ion-gun

A simple low-energy gas ion-gun (Hall et al. 1975) has been constructed to enable us to irradiate FIM specimens in-situ as shown in figure 1. In operating the ion-gun, a gas such as $H_2$, He, Ne, Ar or Xe is continously bled through a stainless steel cylindrical plasma chamber held at a positive potential. The gas is ionized in the plasma chamber by a magnetically confined 2 mA beam of 30 to 100 eV electrons emitted from a heated tungsten filament. The ions produced in the plasma chamber are extracted, accelerated and focused onto the FIM specimen which is held at ground potential. The kinetic energy of the ions is simply equal to the plasma chamber potential. The ion-gun can produce a 4 cm diameter beam of 200 to 3000 eV gas ions at current densities of 0.01 to 10 μA cm$^{-2}$ with gas pressures of $3 \cdot 10^{-6}$ to $5 \cdot 10^{-4}$ Torr respectively.

The low-energy ions are used to produce a sea of SIAs by the focused replacement collision sequence (RCS) mechanism. As a result of the RCSs the immobile vacancies remain at the irradiated surface and the SIAs are injected into the bulk of the FIM specimen. This mechanism is the only presently known one capable of producing isolated SIAs. The ion-gun is also used to implant gas atoms, such as hydrogen, in the tip of the FIM specimen.

An experiment testing the performance of the low-energy gas ion-gun was

conducted in which a tungsten specimen maintained at 30 K was irradiated with 275 eV $Ne^+$ ions. After the removal of the damaged surface layer by field-evaporation an isochronal annealing experiment was performed which revealed the presence of SIAs migrating to the surface of the FIM tip as expected (Scanlan, Styris and Seidman 1971a and 1971b, Seidman 1973, Wilson and Seidman 1975, Seidman, Wilson and Nielsen 1975, Seidman, Wilson and Nielsen 1976). This experiment demonstrates the feasability of two avenues of research. First, the range of RCSs can be directly measured and the energy and temperature dependence of the range can be determined. Second, the interaction of impurity atoms with SIAs introduced by low-energy ion-bombardment can be studied using the atom probe.

## 2.4. Ultra-high vacuum system

The use of an UHV system minimizes the interaction of residual gas atoms with the FIM specimen in two important ways. First, it reduces the probability of the formation of metal atom-gas atom complexes and thereby reduces the number of peaks observed in the (m/n) spectra. Second, it reduces the concentration of artifact contrast effects which are produced as a result of impurity gas atom-surface atom interaction [e.g., artifact vacancies (Berger, Seidman and Balluffi 1973) and artifact SIAs (Seidman and Lie 1972, Robinson, Wilson and Seidman 1973)]. This second point is particularly important for our research, since we are very involved in the study of the interaction of both substitutional and interstitial atoms with point defects.

The primary vacuum pumps are a large titanium sublimation pump (TSP) and a 140 l $sec^{-1}$ ion pump. The vacuum chamber is initially rough pumped by two sorption pumps used in sequence. The use of the TSP, ion pump, and sorption pumps maintains ultraclean conditions and avoids contamination with pump oil. A 5 cm diameter oil diffusion pump is used to pump the main chamber when the atom-probe FIM contains an imaging gas (e.g., helium or neon), since the TSP and ion pumps cannot be used for this purpose. At all other times the diffusion pumps are valved off to prevent possible backstreaming of oil into the vacuum system. Ultimate pressures of $4 \cdot 10^{-10}$ Torr are obtained after baking to 150°C for several hours, while under typical operating conditions the pressure is $1 \cdot 10^{-9}$ Torr.

## 2.5. Specimen exchange device

A specimen-exchange air-lock was incorporated into the design of the atom probe to allow the FIM specimen to be replaced without exposing the vacuum system to atmospheric pressure. For the exchange of a specimen the FIM specimen holder is attached to the end of a 1 m long, 9.5 mm diameter, specimen-exchange rod with a bayonet clip. The specimen exchange rod passes through a Wilson-type sliding

motion feedthrough that is sealed with two viton O-rings. The air lock is rough pumped using two sorption pumps in sequence and is then pumped to $\lesssim 10^{-6}$ Torr by a triode ion pump. Under typical conditions, the pressure in the main chamber remains below $10^{-7}$ Torr during the exchange and drops to $3 \cdot 10^{-9}$ Torr within 15 min after the exchange port has been closed.

2.6. Residual Gas Analyzer

A Uthe Technology Inc. (UTI) Model 100C residual gas analyzer was installed on the atom-probe FIM which allows us to determine the composition of the residual gases in the vacuum system. This instrument has proved to be particularly valuable for determining whether specific impurity atoms originated in the specimen or were artifacts of the vacuum conditions. For example, this instrument has been used to determine the CO and $CO_2$ levels in the vacuum system, thus aiding in the interpretation of the peaks observed at atomic mass 16 which could be due either to titanium in a specimen or oxygen from the vacuum system; oxygen can be produced as a result of the decomposition of CO or $CO_2$ on metal surfaces.

3. Time-of-flight mass spectrometer

To determine the (m/n) values of the pulse-field evaporated ions the voltage on the specimen is measured by an analog-to-digital (A/D) converter and the TOFs of the ions are measured by a digital timer (Berger 1973). The TOF and voltage data is sent to the computer which then calculates the mass-to-charge ratios (m/n) employing the equation

$$m/n = 2e(V_{dc} + \alpha V_{pulse})(t - t_o)^2/d^2 \quad , \qquad (1)$$

(Panitz, McLane and Müller, 1969) where e is the charge of the electron, $V_{dc}$ is the steady-state imaging voltage, $V_{pulse}$ is the evaporation pulse voltage, $\alpha$ is the so-called pulse factor, d is the flight distance, and $(t - t_o)$ is the actual TOF of the ion. The quantity t is the observed TOF and $t_o$ is the total delay time. The controls of the dc, pulse, and focusing lens power supplies are coupled together so that the pulse and lens voltages are always a constant fraction of the dc voltage; this technique simplifies the calibration procedure and optimizes the resolution of the atom probe as discussed by Wagner, Hall and Seidman (1975).

Typically the pulse voltage is maintained at 0.04 to 0.20 of $V_{dc}$ and the lens is maintained at 0.3 to 0.5 of $V_{dc}$. Below approximately 0.04 of $V_{dc}$ the pulser behaves erratically and the continuous dc field-evaporation rate becomes comparable to the pulse-field evaporation rate. Above 0.20 of $V_{dc}$ the increased spread in the energy of the field-evaporated ions degrades the mass resolution of the spectrometer.

3.1. Specimen voltage system

The voltage on the specimen must be precisely controlled and measured if accurate (m/n) values are to be obtained employing equations (1) or (3). The FIM specimen is connected to a CPS 100R, 30 kV power supply through a 10kΩ blocking resistor. A 20 nsec long high-voltage evaporation pulse ($V_{pulse}$) with a rise time of $\leq$0.2 nsec produced by a modified Cayuga Associates CA101 mercury-relay pulser is coupled to the specimen through a 30 kV 4.7 nF capacitor. A Spellman RHR 10PN100 high voltage dc power supply is used to provide the high voltage to the pulser. The values of $V_{dc}$ and $V_{pulse}$ are measured employing an Analogic 5800 series, 13 bit, 16 channel A/D converter. The outputs of the high voltage power supplies are reduced by precision voltage dividers (Hall et al. 1975) to bring these voltages within the 10 V maximum range of the A/D converter.

The high-voltage power-supplies, the voltage dividers, and the A/D converter were tested by monitoring the measured voltage with the aid of the computer and comparing it with the known voltage obtained using a high precision Hewlett-Packard 3439A digital voltmeter. These tests indicated that the measured voltages are accurate to within 5 volts (which corresponds to one bit in the A/D converter) and that the voltages are stable to within $\leq$5 volts over periods of several hours.

3.2. Chevron ion detector

The ion detector at the downstream end of the flight tube consists of two 25 mm diameter CEMAs in the Chevron configuration and a phosphor screen (Colson, McPherson and King, 1973). The 37.5 μm diameter channels in the first CEMA are at an angle of 5° with respect to the normal to the front surface of the CEMA to prevent secondary ion feedback through both CEMAs. Behind the two CEMAs is a 25 mm diameter phosphor screen which is capacitively coupled to a LeCroy Research System (LRS) 133B dual amplifier operated at a gain of 25. The output pulse from the amplifier is delayed 500 nsec (by ∿150 m of RG 58 cable) and then triggers one channel of an LRS 161 discriminator which stops the digital timer. The Chevron detector was chosen because its particle detection characteristics are good (Brenner and McKinney 1972, Müller, Krishnaswamy and McLane 1973) and it provides a visible image of the ion beam which is extremely useful for the alignment and focusing of the TOF mass spectrometer.

If small concentrations of impurity atoms or alloying elements are to be reliably detected the Chevron ion detector must be well characterized with respect to spurious output pulses. Tests of our detector indicate that the random background count rate is ∿10 $sec^{-1}$ which indicates that impurity atom concentrations in the 10 appm range can be detected. The occurrence of artifact pulses following the true pulse by up to 10 μsec is <0.2%.

3.3. Digital timer

The digital timer that we have constructed can measure TOFs as long as 99.00 μsec of up to eight consecutive field evaporated ions with an accuracy of 0.01 μsec. The basic features of this timer are described in an earlier paper (Berger 1973). The version presently being used has a number of modifications which were introduced to improve the accuracy and reliability of the timer; the principle modification being that the start signal from the pulser and the stop signals from the Chevron ion detector are synchronized with the timer's clock so that problems caused by changes of logic state during clock transitions are completely eliminated. To test the digital timer pulses with known relative delays were measured and checked by the computer. In over $10^6$ operations no errors have been detected, with the modified timer, indicating that the TOFs measured during experiments can be treated with confidence (Hall et al. 1975).

3.4. Resolution of the TOF mass spectrometer

The resolution of the TOF atom probe has been discussed at length in the literature (e.g., see Müller and Krishnaswamy 1974 and Regan, Turner and Southon 1976). There are three major factors affecting the resolution: (1) inaccurate determination or variations of the calibration parameters $\alpha$, $t_o$ and d; (2) uncertainty in the measurement of the TOFs and the voltage on the specimen; and (3) energy deficits.

By maintaining $V_{pulse}$ at a constant fraction (f) of $V_{dc}$ so that

$$V_{pulse} = f\, V_{dc} \tag{2}$$

equation (1) becomes

$$m/n = (2e/d_{eff}^2)\, V_{dc}\, (t - t_o)^2 \tag{3}$$

where

$$d_{eff} = d/(1 + \alpha f)^{1/2} = \text{constant} \quad . \tag{4}$$

This technique reduces the number of calibration parameters to two, namly $d_{eff}$ and $t_o$ thus eliminating the need for an accurate, independent determination of $\alpha$. Furthermore, the calibration parameters $\alpha$ and d now only affect the absolute values of (m/n) and thus inaccuracies in their determination do not affect the mass resolution ($\Delta m/m$) of the atom probe. The remaining calibration parameter $t_o$ can be measured electronically to a high degree of accuracy and poses no problem. In all of our work to date, we have never found the basic shape of the spectrum to depend on the exact determination of the calibration parameters. Both $\alpha$ and $t_o$ can be held constant if high quality, low drift electronics are employed. Thus the only remaining factors which affect the resolution are the uncertainties

in the TOF and voltage measurement, variations in d and energy deficits.

For our mass spectrometer with a time uncertaintly of ± 10 nsec, a voltage uncertainty of ± 3 V and a flight path length variation of $\lesssim \pm 0.05$ mm a standard calculation of the (m/n) uncertainty for $^{186}W^{+3}$[m/n) = 62 amu] with total voltage $(V_{dc} + \alpha V_{pulse})$ of 15 kV and d = 1600.3 mm predicted a full width at half maximum (FWHM) of $\lesssim 0.20$ amu and a full width at 0.1 maximum of $\lesssim 0.34$ amu. The measured FWHM for $^{186}W^{+3}$ (see figure 3(a) in Hall et al. 1976) was 0.2 amu while the full width at 0.1 maximum was 0.7 amu; the first criterion yields a $\Delta m/m$ value of $\sim 1/300$ while the latter criterion yields a $\Delta m/m$ value of $\sim 1/90$.

The observed FWHM value is in good agreement with the predicted value while the observed full width value at 0.1 maximum is considerably greater than the predicted value. All of the peaks we have observed to date were sharp on the leading edge with a tail extending to the high mass side of each peak (e.g., see figure 2 in Hall et al. 1976 for the $Mo^{+2}$ spectrum and figures 5, 7, 8 and 9 in this paper). This large tail contributes strongly to the observed full width at 0.1 maximum value and only weakly to the FWHM value. The observation of this high mass tail appears to be quite general for all straight TOF atom probes and has been attributed to energy deficits associated with the field evaporation process (Müller 1971, Krishnaswamy and Müller 1974). In addition, Regan, Turner and Southon (1976) have also analyzed the energy deficit problem in terms of pulse shape and the decay behavior of the evaporation pulse. At present the best approach to eliminate energy deficits, and thereby increase the $(\Delta m/m)$ value to $\sim 1/1000$, appears to be through the use of the isochronous focusing lens designed by Poschenrieder (1972) and adopted by Müller and Krishnaswamy (1974) to the atom probe. We emphasize strongly that the straight TOF atom probe has a resolution which is sufficient for the study of a wide range of materials. For example, the practical resolution of our instrument is clearly $\sim 1/200$ since we have resolved the five stable isotopes of W ($^{180}W$, $^{182}W$, $^{183}W$, $^{184}W$ and $^{186}W$) and the two stable isotopes of Re ($^{185}Re$ and $^{187}Re$) in a W-25 at.% Re alloy [see figure 3(a) and (b) in Hall et al. 1976]. Furthermore, the results presented in Section 5 amply demonstrate the adequacy of the resolution of the straight TOF atom probe.

## 4. Computer system

The atom probe has been interfaced to a Nova 1220 minicomputer which, in the course of an experiment, can collect, store, and analyze the mass spectrometer data. The computer system hardware consists of: (1) a Data General Nova 1220 minicomputer with 32 K words of memory; (2) three Data General magnetic cassette tape transports; (3) a Tektronix 4010 graphics display terminal and 4610 hard copy unit; and (4) an ASR33 Teletype. The computer system interacts with the

atom probe via an Analogic 5800 series A/D converter, which is used to measure the specimen voltage, and a specially constructed interface which allows the computer to trigger the high voltage pulse to the specimen and to read in the TOFs from the digital timer. With the aid of this automated system we can presently record and analyze 600 TOF events $min^{-1}$.

4.1. Computer program to operate the atom probe

A program called the Atom Probe Operating System (APOS) is used when the computer is controlling the atom probe. This program is written in BASIC and ASSEMBLY languages and incorporates many interactive features which allow the operator to continuously monitor the performance of the atom probe during an experimental run. The principle features of this program can be described most easily by listing the sequence of events that take place in a typical experiment. After certain variables have been initialized, such as the calibration parameters, the computer initiates the pulsing of the FIM tip. As the FIM specimen is field evaporated the voltage is slowly raised by the operator to maintain a steady pulse evaporation rate as monitored by an audio ratemeter. After each pulse the computer reads in the TOF and voltage data, computes the (m/n) values, increments the appropriate bin of the histogram by one, and then stores the data on magnetic cassette tape. When sufficient data has been accumulated in the histogram it is displayed on the graphics display terminal. The information on the cassette tape can be read back to reproduce the histogram or to produce a composition profile showing the cumulative number of atoms of a given type within a specified (m/n) range as a function of the total number of atoms detected.

A schematic illustration of the physical principle behind a composition profile is illustrated in figure 3. Figure 3(a) shows a FIM tip formed from a solid solution alloy consisting of a solvent A and a solute B. The tip contains a precipitate which is rich in B; the solute atoms are denoted by the solid black circles. The tip-to-image intensification system distance is adjusted so that during the course of the pulse-field evaporation of the specimen all the atoms (A and B) contained within the indicated cylindrical volume element are chemically analyzed by the atom probe. Figure 3(b) shows the corresponding composition profile; the number of B atoms versus the cumulative number of A plus B atoms. The cumulative number of atoms is proportional to depth (z), since the specimen is chemically analyzed by disecting atomic planes sequentially; in a typical experiment the specimen is analyzed to a depth of 250 A. If the B atoms are distributed uniformly† the average slope of the plot in the regions away from the indicated

† A random distribution of the elements A and B will, of course, also exhibit

compositional fluctuation effects; we discuss this point further in Section 5. We will use the word uniform to indicate an absence of any gross segregation effects over the range of space that we sample.

---

precipitate determines the average composition of the alloy. In the region of the precipitate the average slope of this plot yields the precipitate's average composition. In this example we have specifically used a precipitate to illustrate the concept of a composition profile, since in the case of a precipitate a fraction of the solute atoms have been removed from the solid solution. The identification of this change in composition as being caused by a precipitate can, in practice, be confirmed from the microstructural information present in the FIM image.

4.2. Auxilliary programs

A number of auxilliary programs have been developed which contribute to the interpretation of the experimental results and to the maintenance of the atom probe. The DICTIONARY GENERATING program prepares an ordered table of (m/n) values for selected combinations of elements and is used as an aid in identifying the observed peaks in the measured (m/n) spectra. SYNGEN is a synthetic data generating program which produces simulated (m/n) spectra. This program has been useful in studying the effect of uncertainties in the TOF and voltage values on mass resolution. In order to insure the reliable operation of the atom probe an extensive set of diagnostic programs have also been developed. These programs are used periodically to test the performance of the computer, the cassette drive, the atom probe interface and the high-voltage pulser.

5. Some experimental results

In this section we report on the chemical analysis of a number of pure metals and alloys by the atom-probe technique. The materials that were examined included tungsten, molybdenum, tungsten-(rhenium), molybdenum-(titanium), molybdenum-(titanium and zirconium)†, a special low-swelling stainless steel alloy (LS1A)

---

† Commonly called TZM.

---

and an iron-based metallic glass (Metglas 2826). The results of the experiments on these materials demonstrated that they could be chemically analyzed quantitatively and that more detailed experimental investigations of irradiation produced defects in them should be reasonably straightforward.

Before presenting the experimental results we wish to briefly discuss the use of the word clustering as it is very germane for our results on alloys. In the theory of solid solutions (e.g., see Christian 1965a) the term clustering has a very exact meaning. Specifically, clustering (or negative short-range order) implies that <u>like</u> atoms have a greater than random probability of being nearest

neighbors of one another; this behavior is indicative of a miscibility gap, at lower temperatures, on a phase diagram. Alternatively, short-range order (i.e., anti-clustering) implies that unlike atoms have a greater than random probability of being nearest neighbors of one another; this behavior is indicative of a disorder-order transformation, at lower temperatures, on a phase diagram. Furthermore, a random solid solution will exhibit composition fluctuations and the root-mean-square deviation $[\sqrt{(\Delta x)^2}]$ from the average composition [in atom fraction of the solute (x)] is given by $[x(1 - x)/n]^{1/2}$ where n is the total number of atoms involved in the fluctuation. Since we are dealing with small sample sizes the probability of seeing a local composition fluctuation is high and, indeed, our composition profiles do exhibit these composition fluctuations (e.g., see the profile for $Ti^{+3}$ shown in figure 6). The total sample size can be quite large; for example, it is possible to obtain a composition profile of $10^5$ atoms. By small sample size we mean a small volume of space within the total sample volume which can contain only a single atom if so desired. The term cluster is also used, for example, in discussing Guinier-Preston (G-P) zones (e.g., see Christian 1965b) where "precipitation is preceded by the formation of coherent clusters rich in solute atoms within the parent lattice". The G-P zones are metastable clusters which are <u>not</u> a separate phase of the system. With the atom-probe technique it is possible to observe this pre-precipitation phenomenon. Finally, we come to a precipitate which represents a separate phase of the system (independent of whether it is stable or metastable). The FIM image can be used, in conjunction with the composition profile, to definitively identify a precipitate and hence to distinguish it from: (1) clustering; (2) short-range order (or anti-clustering); (3) composition fluctuations; or (4) pre-precipitation clusters such as G-P zones.† In this section we use the term cluster to indicate any local composition fluctuation which is obviously greater than the composition fluctuations expected in a random solid solution; although, in principle, it is possible to make the distinctions enumerated above.

† A more detailed discussion of clustering is to be published in the future.

5.1. Pure metals (tungsten and molybdenum)

The spectra of $W^{+3}$ and $W^{+4}$, and $Mo^{+2}$ have been published earlier (Wagner, Hall Seidman 1975, Hall et al. 1976). The spectrum of $W^{+3}$ clearly shows the five stable isotopes of W ($^{180}W$, $^{182}W$, $^{183}W$, $^{184}W$, and $^{186}W$) and the measured isotopic abundances were in good agreement with the handbook values. In the $Mo^{+2}$ spectrum we very clearly resolved the seven stable isotopes of Mo ($^{92}Mo$, $^{94}Mo$, $^{95}Mo$, $^{96}Mo$, $^{97}Mo$, $^{98}Mo$ and $^{100}Mo$) and we also obtained isotopic abundances which agreed very well with the handbook values (Hall et al. 1975).

5.2. Tungsten - (25 at.% rhenium) alloy

The results on W (see Section 5.1) and W-25 at.% Re will serve as a control for some in-progress experiments on fast-neutron irradiated specimens of these same materials. Pure W exhibits considerable swelling (void formation) as a result of fast-neutron irradiation at ∿0.4 to 0.6 of the absolute melting temperature and the addition of Re to W strongly suppresses this swelling (e.g., Moteff, Sikka and Jang 1975). It is our objective to determine how the Re is re-distributed as a result of the fast-neutron irradiation treatment in an effort to determine the mechanism(s) for the suppression of void formation.

An FIM specimen was prepared from off the spool W-25 at.% Re thermocouple wire; its (m/n) spectrum has been previously published (Hall et al. 1976). Figure 4 shows the composition profiles for the two stable Re isotopes ($^{185}$Re and $^{187}$Re). This experiment demonstrated that the Re isotopes can be distinguished from the immediately adjacent W isotopes ($^{184}$W and $^{186}$W). The average composition of the rhenium determined for the $^{185}$Re isotope was 10.6 at.% and for the $^{187}$Re isotope it was 14.8 at.%; hence, the overall composition was 25.4 at.% Re as determined from the average slopes of the profiles shown in figure 4. The rhenium concentration was also found by a least squares analysis of the atom probe data to be 22 ± 2 at.% which agrees with the nominal concentration of 25 at.%. The first conclusion drawn from this experiment was that a Re concentration of 25 at.% or higher could be easily detected in tungsten. A second conclusion is that the vast majority of the Re atoms were in solid solution in this specimen; this conclusion was based on the fact that the measured Re concentration was approximately equal to the nominal composition of the alloy and also that the FIM image showed no evidence for precipitation. A third conclusion is that there was no evidence for any pre-precipitation. A fourth conclusion is that the composition profiles exhibit composition fluctuations about the average Re isotope compositions. To date we have been unable to conclude whether or not there is any evidence for short-range order (anti-clustering) obtainable from the composition profiles.

5.3. Molybdenum - (titanium) alloy

The Mo - 1.0 at.% Ti alloy exhibits an enhanced swelling behavior when compared to the molybdenum specimens irradiated under identical conditions to the same fast neutron dose (Moteff, Sikka and Jang 1975). It is the purpose of the present experiment to determine the role played by the titanium in the swelling enhancement behavior of neutron irradiated Mo(Ti). It is interesting to note, by contrast, that Johnston et al. (1976) have found Ti to be a particularly effective swelling inhibitor in a series of model Fe-Cr-Ni alloys.

Atom-probe FIM experiments were performed on unirradiated specimens of a Mo-1.0 at.% Ti alloy; the results will serve as a control for a series of experiments on neutron irradiated Mo-1.0 at.% Ti. The alloy was originally swaged from reroll stock which had been recrystallized at 1090°C and then hot drawn to a 1.5 mm diam. between 815 and 980°C. A wire specimen was prepared from the 1.5 mm diam. rod by thinning it electrolytically to a 0.2 mm diam. using a solution which consisted of 25 parts $H_2SO_4$ to 175 parts $CH_3OH$ (by volume). The FIM specimens were prepared by the dipping technique at 5 VaC in a solution of 1 part $H_2SO_4$: 4 parts HCl: 8 parts $CH_3OH$ (by volume).

The $Ti^{+3}$ spectrum for the as-received Mo-1.0 at.% Ti alloy is shown in figure 5. The five isotopes of Ti ($^{46}Ti$, $^{47}Ti$, $^{48}Ti$, $^{49}Ti$ and $^{50}Ti$) are very clearly seen in this figure. Table 1 shows a comparison of the experimental $Ti^{+3}$ isotopic abundances with the actual isotopic abundances. The agreement is reasonable considering that the sample size only involved 30 $Ti^{+3}$ ions for all five siotopes. The five $Ti^{+3}$ isotopes present a very decisive indicator of Ti which allows us to distinguish it from O; oxygen has only three isotopes ($^{16}O$, $^{17}O$, $^{18}O$) with $^{16}O$ having a natural abundance of 99.8 at.% of the three O isotopes. The concentration of Ti was determined to be 0.28 at.% this represents 28% of the nominal Ti concentration. There may also be additional Ti atoms which field evaporate in the +2 charge state and they would therfore be superimposed on the $Mo^{+4}$ portion of the spectrum. However it is emphasized that Chang and Perlmutter (1963) have shown that $Mo_2C$, TiC and ZrC precipitates can form in both Mo(Ti) and TZM. Thus the remaining 72% of the Ti may alternatively be tied up in the form of TiC precipitates which exist at a number density that is below the limit of detection of the FIM technique. The Ti observed was also found to be uniformly distributed throughout the alloy without any gross clustering effects. This is significant because a comparison of the present results with the results on the irradiated Mo(Ti) alloys should allow us to comment in detail on the changes produced in the spatial distribution of Ti atoms in the alloy as a result of the fast neutron irradiation.

The Mo(Ti) spectrum was recorded with the atom probe at a background pressure of $5.2 \cdot 10^{-10}$ Torr and at a tip temperature of 42 K. The major residual gas components were $H_2$ ($4.73 \cdot 10^{-10}$ Torr), He ($0.02 \cdot 10^{-10}$ Torr), $CH_4$ ($0.17 \cdot 10^{-10}$ Torr), CO ($0.24 \cdot 10^{-10}$ Torr), and $CO_2$ ($0.04 \cdot 10^{-10}$ Torr). The voltage range was $V_{dc}$ = 5,600 to 9,400 V, the value of f was 0.05, and the calibration parameters were $\alpha = 1.2$, $t_o = 0.56$ µsec, and d = 2218 mm.

5.4. Molybdenum - (titanium and zirconium) alloy (TZM)

The alloy Mo-1.0 at.% Ti-0.08 at.% Zr (TZM) had been found to exhibit an enhanced swelling behavior and a very fine dislocation substructure when compared

to molybdenum for fast neutron irradiation temperatures of less than 650°C (Eyre 1972). At present we are engaged in a study to determine the role(s) played by the Ti and Zr additions to Mo in causing this swelling enhancement. The atom probe data on TZM presented in this section will serve as a control for our experiments on fast-neutron irradiated TZM specimens.

The 0.2 mm diam. wire FIM specimens were cold-drawn from a 1 mm diam. rod of TZM which had been stress-relieved between 870 and 980°C. After the cold-drawing operation the wire specimens were brittle and somewhat fibrous. The FIM specimens were prepared by the dipping technique in the electropolishing solution used for the Mo-1.0 at.% Ti alloy.

Figure 6 shows a semilogarithmic plot of the (m/n) histogram† of TZM between 0 and 55 amu. The peaks near 24, 32 and 48 amu are associated with $Mo^{+4}$, $Mo^{+3}$ and $Mo^{+2}$ respectively. The cluster of peaks near 16 amu are associated with $Ti^{+3}$ ($^{46}Ti$, $^{47}Ti$, $^{48}Ti$, $^{49}Ti$, $^{50}Ti$) and they correspond to a Ti concentration of 0.26 at.% this represents 26% of the nominal Ti concentration. The comments made in Section 5.3. with respect to the difference between the measured and the nominal Ti concentration in the Mo(Ti) alloy also apply to TZM. The peaks at 30 and 45 amu are associated with $^{90}Zr^{+3}$ and $^{90}Zr^{+2}$ respectively and correspond to a total Zr concentration of 0.13 at.% which is in reasonable agreement with the nominal Zr concentration.

† For figures 6, 8 and 9 we employed semilogarithmic plots for the histograms because of the large number of field-evaporated ions detected. This type of plot tends to emphasize the random background events; in reality the random events only constitute a very small fraction of the total number of ions detected.

The spatial distribution profiles of Ti and Zr are shown in figure 7; each step in the ordinate scale corresponds to a single Ti or Zr atom. The Ti atoms observed were distributed uniformly throughout the specimen and they did not exhibit any gross clustering effects. By comparison all the Zr atoms detected were contained in a single cluster. This Zr cluster was detected just before the FIM tip failed and it certainly may have contributed to the failure of the tip. These control experiments on TZM demonstrated that both the Ti and Zr alloying elements in the <0.5 at.% range could be detected in Mo and that the techniques developed to date should work reasonably well for irradiated specimens.

With the exception of a few events in the range from 1 amu to 6 amu (which are associated with H, He, and C) the spectrum shows a very clean background. The TZM spectrum was recorded with the atom probe at a background pressure of $4.5.10^{-10}$ Torr and at a tip temperature of 35 K. The major residual gas components

were $H_2$ ($4.22 \cdot 10^{-10}$ Torr), $CH_4$ ($0.08 \cdot 10^{-10}$ Torr), CO ($0.18 \cdot 10^{-10}$ Torr), and $CO_2$ ($0.03 \cdot 10^{-10}$ Torr). The voltage range was $V_{dc}$ = 12,200 to 13,300 V, the value of f was 0.05, and the calibration parameters were $\alpha$ = 1.2, $t_o$ = 0.56 μsec, and d = 2218 mm.

5.5. Low swelling stainless steel alloy (LS1A)

A low swelling stainless steel alloy (LS1A) developed at the Oak Ridge National Laboratory (ORNL) by Bloom et al. (1976), has been analyzed by the atom-probe FIM technique. To date we have restricted our work to unirradiated specimens of this alloy because of the high radioactivity of the neutron irradiated specimens. The alloy LS1A contains 2.06 at.% Si and 0.16 at.% Ti as swelling inhibitors. It is the purpose of the present study to determine the role played by these swelling inhibitors. The material was examined in the cold-worked state after having been drawn from a 0.24 mm to a 0.20 mm diam. wire. After each drawing pass, except the last one, the material was annealed at 1050°C for 15 minutes in an argon atmosphere. The FIM specimens were prepared by the dipping technique at 10 Vdc in an electropolishing solution consisting of 33% $H_3PO_4$ in $H_2O$.

Table 2 shows the composition of each element in this alloy as determined by the atom-probe FIM technique. The first column in the table gives the average composition as determined by the atom-probe technique. It is seen that the basic agreement is good. All the alloying elements (Fe, Cr, Ni, Mn, Mo, C, Si, and Ti) in LS1A were readily identified by the atom-probe FIM technique as shown in firure 8. In particular the isotopes $^{52}Cr^{+4}$, $^{28}Si^{+2}$, $^{29}Si^{+2}$, $^{30}Si^{+2}$ and $^{48}Ti^{+3}$ can be easily seen in the 12 to 17 amu part of the spectrum. The $^{48}Ti^{+3}$ peak at 16 amu could contain an undetermined amount of oxygen. The most probable source of the oxygen is residual CO and $CO_2$ in the FIM which can decompose on the surface of the FIM tip. The isotopes $^{50}Cr^{+2}$, $^{52}Cr^{+2}$, $^{54}Fe^{+2}$, $^{55}Mn^{+2}$, $^{56}Fe^{+2}$, $^{58}Ni^{+2}$ and $^{60}Ni^{+2}$ can be clearly identified in the 24 to 34 amu portion of the spectrum. In addition, an analysis of the spatial distribution of each alloying element revealed the existence of a cluster consisting of three nickel atoms, three silicon atoms, two carbon atoms, two titanium atoms, two molybdenum atoms, one manganese atom and one iron atom (see last column of Table 2). It is highly improbable for such a cluster to form as the result of a simple statistical fluctuation.

The spectrum for the LS1A alloy was recorded with the atom-probe FIM at a background pressure of $1 \cdot 10^{-9}$ Torr and at a tip temperature of ∿50 K. The voltage range was from $V_{dc}$ = 16,600 to 19,900 V, the value of f was 0.075 and the calibration parameters were $\alpha$ = 1.482, $t_o$ = 0.56 μsec and d = 2227 mm.

5.6. Iron-based metallic glass (Metglas 2826)

A metallic glass, known commercially as Metglas 2826 and sold by Allied Chemical Corporation, with a nominal composition of 40 at.% Fe, 40 at. % Ni,

14 at.% P and 6 at.% B was examined by the atom probe technique; see Masumoto and Maddin (1975) for a review of work on the structural stability and mechanical properties of metallic glasses. The experiments were performed to establish the feasability of studying the clustering behavior of the phosphorous and boron in this alloy. The clustering of phosphorous had been suggested as a possible mechanism for the embrittlement of this alloy following heat treatment below its crystallization temperature. Prior to the atom-probe examination the specimen was annealed at 150 to 170°C for ∿6 h (a standard UHV bake out of the FIM). The FIM specimens were prepared in an electropolishing solution which consisted of 4 parts ethanol; 1 part perchloric acid (by volume).

The (m/n) spectrum for Metglas 2826 in figure 9 shows that the various constituents can be easily identified. The composition as determined by an atom probe analysis is 35.8 ± 1.3 at.% Fe, 37.1 ± 1.3 at.% Ni, 20.9 ± 1.0 at.% P and 6.2 ± 0.5 at.% B; the spatial distribution of B and P in this specimen is plotted in figure 10. The composition values for the elements Fe, Ni and B are in reasonable agreement with the nominal composition supplied by Allied Chemical Corporation. In the case of P the composition as determined by the atom-probe technique is ∿1.5 times greater than the nominal composition. A statistical analysis of this data shows no obvious evidence for the clustering of the B and P. There are two possible explanations for our observation: (1) the nominal composition determined by the manufacturer is incorrect for the material we used; and (2) the region of space sampled in our experiment was occupied by a cluster which is rich in P. Future experiments on other specimens heated to other temperatures will be used to determine the annealing conditions under which clustering starts.

The Metglas 2826 data were recorded in the presence of $10^{-7}$ Torr Ne, at a background pressure of $2.5 \cdot 10^{-9}$ Torr and at a tip temperature of 63 K. The voltage range ($V_{dc}$) was varied between 18,500 to 19,400 V, the value of f was 0.10 and the calibration parameters were $\alpha = 1.482$, $t_o = 56$ μsec and d = 2231 mm.

5.7. Conclusions

The experiments reported in Section 5 on pure metals, simple alloys, a complex commercial steel and a metallic glass alloy clearly demonstrate the capability of our computer controlled UHV atom-probe to chemically analyze these materials in a rapid and quantitative manner. Specifically we have obtained the following results: (1) resolved the five stable isotopes of tungsten and measured isotopic abundances which are in agreement with the handbook values; (2) resolved the seven stable isotopes of molybdenum and measured isotopic abundances which are in good agreement with the handbook values; (3) resolved the two stable isotopes of rhenium from the five stable isotopes of tungsten in a W-25 at.% Re alloy and determined the compo-

sition profiles for the Re isotopes; (4) resolved the five stable isotopes of titanium in a Mo-1.0 at.% Ti alloy and showed that the Ti remaining in solid solution was distributed uniformly throughout the specimen; (5) determined the composition profiles of titanium and zirconium in a Mo-1.0 at.% Ti-0.08 at.% Zr (TZM) alloy and showed that the Ti remaining in solid solution was distributed uniformly whereas the Zr was found to be non-randomly distributed; (6) identified and determined the concentration of all the alloying elements in a special low swelling 316 stainless steel (LS1A) and also detected a cluster consisting of 3 Ni atoms, 3 Si atoms, 2 C atoms, 2 Ti atoms, 2 Mo atoms, 1 Mn atom and 1 Fe atom; and (7) analyzed a Metglas 2826 specimen which had been annealed at 150 to 170°C for ~6 h and found its composition to be 35.8 ± 1.3 at.% Fe, 37.1 ± 1.3 at.% Ni, 20.9 ± 1.0 at.% P and 6.2 ± 0.5 at.% B.

Acknowledgements

We are indebted to Dr. S. S. Brenner of the U. S. Steel Corporation for the plans of the goniometer stage and for helpful advice and discussions concerning the TOF atom-probe FIM technique. We are grateful to Mr. R. Whitmarsh, Mr. J. Hart, and Mr. A. Babbaro for technical assistance and Prof. R. W. Balluffi for encouragement. We also wish to thank Mr. C. Mooney of AMAX Speciality Metals for a rod of the Mo-1 at.% Ti-0.08 at.% Zr alloy, Professor J. Moteff of the University of Cincinnati for several rods of Mo-1 at.% Ti alloy, Drs. E. E. Bloom, J. O. Stiegler and L. K. Mansur of the Oak Ridge National Laboratory for wire specimens of the low-swelling stainless steel (LS1A), and Drs. J. Walter and P. Rao of the General Electric Research and Development Laboratory for introducing us to the metallic glass embrittlement problem, the Metglas 2826 specimens and for help in preparing FIM specimens of this alloy.

References

Andren H-O and Norden H 1975 22nd Intern. Field Emission Symposium, Georgia Institute of Technology

Berger A S 1973 Rev. Sci. Instrum. 44 592-94

Berger A S, Seidman D N and Balluffi R W 1973 Acta Met. 21 123-36

Bloom E E, Stiegler J O, Rowcliffe A F and Leitnaker J M 1976 Scripta Met. 10 303-08

Brenner S S and Goodman S R 1971 Scripta Met. 5 865-69

Brenner S S and McKinney J T 1968 Appl. Phys. Lett. 13 29-32

—— 1970 Surf. Sci. 23 88-111

—— 1972 Rev. Sci. Instrum. 43 1264-67

Chang W H and Perlmutter I 1963 High Temperature Materials (New York: Interscience) pp 347-70

Chambers R S and Ehrlich G 1975 22nd Intern. Field Emission Symposium, Georgia Institute of Technology

Christian J W 1965a The Theory of Transformations in Metals and Alloys (Oxford: Pergamon) pp 217-22

—— 1965b The Theory of Transformations in Metals and Alloys (Oxford: Pergamon) pp 606-17

Colson W B, McPherson J and King F T 1973 Rev. Sci. Instrum. 44 1694-96

Eyre B L 1972 Proc. Discussion Meeting on Defects in Refractory Metals eds. R DeBatist, J Nihoul and L Stals (Mol, Belgium: SCK/CEN) pp 311-50

Gallot J, Sarrau J and Bostel A 1975 Le Vide 179 173-81

Goodman S R, Brenner S S and Low J R 1973a Met. Trans. 4 2363-69

—— 1973b Met. Trans. 4 2371-78

Hall T M, Wagner A, Berger A S and Seidman D N 1975 Cornell University Materials Science Center Report No. 2357

—— 1976 Scripta Met. 10 485-88

Johnston W G. Lauritzen T, Rosolowski J H and Turkalo A M 1976 General Electric Report No. 76CRD019, Schenectady, New York

Kinosita K, Nakamura S and Kuroda T 1974 Japan J. Appl. Phys. 13 1775-79

Krautz E, Ladurner J and Leisch M 1976 23rd Intern. Field Emission Symposium, Pennsylvania State University

Krishnaswamy S V, McLane S B and Müller E W 1974 J. Vac. Sci. Technol. 11 899-902

Krishnaswamy S V and Müller E W 1974 Rev. Sci. Instrum. 45 1049-52

Lewis R J and Smith G D W 1975 22nd Intern. Field Emission Symposium, Georgia Institute of Technology

Masumoto T and Maddin R 1975 Mater. Sci. Eng. 19 1-24

Moteff J, Sikka V K and Jang H 1975 Physics of Irradiation Produced Voids ed R S Nelson (London: Her Majesty's Stationary Office) pp 181-87

Müller E W 1971 Ber. Bunsenges. Phys. Chem. 75 979-87

Müller E W, Krishnaswamy S V and McLane S B 1973 Rev. Sci. Instrum. 44 84-6

Müller E W and Krishnaswamy S V 1974 Rev. Sci. Instrum. 45 1053-59

Müller E W, Panitz J A and McLane S B 1968 Rev. Sci. Instrum. 39 83-6

Müller E W and Tsong T T 1973 Progress in Surface Science Vol. 4 ed S G Davison Oxford: Pergamon Press) pp 1-139

Panitz J A 1975 CRC Critical Reviews in Solid State Physics (Cleveland: CRC) pp 153-79

Panitz J A, McLane S B and Müller E W 1969 Rev. Sci. Instrum. 40 1321-24

Poschenrieder W P 1972 Int. J. Mass Spectrom. Ion Phys. 9 357-73

Regan B J, Turner P J and Southon M J 1976 J. Phys. E: Sci. Instrum. 9 187-93

Robinson J T, Wilson K L and Seidman D N 1973 Phil. Mag. 27 1417-32

Rosebury F 1965 Handbook of Electron Tube and Vacuum Techniques (New York: Addison-Wesley) pp 250-53

Scanlan R M, Styris D L and Seidman D N 1971a Phil. Mag. 23 1439-57

—— 1971b Phil. Mag. 23 1459-78

Seidman D N, Scanlan R M, Styris D L and Bohlen J W 1969 J. Phys. E: Sci. Instrum. 2 473-76

Seidman D N and Lie K H 1972 Acta Met. 20 1045-60

Seidman D N 1973 J. Phys. F: Metal Phys. 3 393-421

Seidman D N, Wilson K L and Nielsen C H 1975 Phys. Rev. Lett. 35 1041-42

—— 1976 Fundamental Aspects of Radiation Damage in Metals eds M T Robinson and F W Young (Springfield, Virginia: National Technical Information Service) pp 373-96

Turner P J et al. 1969 J. Sci. Instrum. 2 731-33

Turner P J and Papazian J M 1973 Met. Sci. J. 7 81-86

Turner P J, Regan B J and Southon M J 1973 Surf. Sci. 35 336-44

Wagner A, Hall T M and Seidman D N 1975 Rev. Sci. Instrum. 46 1032-34

Watts A J and Ralph B 1975 22nd Intern. Field Emission Symposium, Georgia Institute of Technology

Wilson K L and Seidman D N 1975 Rad. Effects 27 67-74

Table 1. Comparison of the experimental $Ti^{+3}$ isotopic abundances in an as-received Mo-1.0 at.% Ti alloy with the actual isotopic abundances.

| Isotope | Number of Atoms (N) | Experimental† % | Actual % |
|---|---|---|---|
| $^{46}Ti$ | 4 | 13 ± 7 | 7.9 |
| $^{47}Ti$ | 1 | 3 ± 3 | 7.3 |
| $^{48}Ti$ | 18 | 60 ± 14 | 73.9 |
| $^{49}Ti$ | 4 | 13 ± 7 | 5.5 |
| $^{50}Ti$ | 3 | 10 ± 6 | 5.4 |
| Totals | 30 | 99 | 100 |

† The ± values were calculated from the $\sqrt{N}/\Sigma N$ values where N is the number of atoms counted.

Table 2. Comparison of the composition of a low swelling stainless steel (LS1A) as determined by chemical analysis and by atom probe FIM analysis for the bulk specimen and for a non-random cluster.

| Element | Chemical analysis (Atomic %) | Atom probe analysis of the bulk specimen (Atomic %)† | Atom probe analysis of a cluster (Number of Atoms) |
|---|---|---|---|
| Fe | 64.0 | 62.2 ± 1.1 | 1 |
| Cr | 17.4 | 14.5 ± 0.5 | 0 |
| Ni | 12.9 | 16.2 ± 0.6 | 3 |
| Mn | 2.0 | 2.6 ± 0.2 | 1 |
| Mo | 1.0 | 1.8 ± 0.2 | 2 |
| C | 0.37 | 0.4 ± 0.1 | 2 |
| Si | 2.1 | 1.7 ± 0.2 | 3 |
| Ti | 0.16 | 0.20 ± 0.06 | 2 |
| Other | 0.15 | 0.5 ± 0.1 | 0 |
| Totals | 100.1 | 100.1 | |

† The uncertainties were calculated from the $\sqrt{N}/\Sigma N$ values were N is the number of atoms counted.

Figure Captions

Figure 1 Schematic diagram of the TOF atom-probe FIM. Shown at the top of the figure are the internal elements of the atom probe including the FIM specimen, the internal image intensification system, the focusing lens, the 45° viewing mirror, the Chevron ion detector and the low energy gas ion gun for performing in-situ irradiations. The digital timer and specimen voltage system shown in the lower part of the figure are operated automatically by a Nova 1220 mini-computer which is interfaced to a Tektronix 4010 graphics display terminal and a 4610 hard copy unit so that data can be plotted on-line during the course of an experiment.

Figure 2 A schematic diagram of the goniometer stage which allows the FIM specimen to be rotated about two mutually orthogonal axes. The liquid-helium cryostat is connected to the specimen mount via a flexible gold braid. The copper radiation shield surrounding the specimen mount is cooled by a second gold braid which is also connected to the liquid helium cryostat.

Figure 3 During the course of an atom-by-atom disection of an FIM specimen by the pulse-field evaporation technique the atom probe determines the distribution of chemical species in an approximately cylindrical volume element of the specimen as shown in 3(a). A plot of the number of B atoms (we consider here the case of a binary alloy consisting of A and B atoms) as a function of the total number of atoms (A plus B) detected yields a composition profile. The presence of a local composition variation produced by a precipitate results in a change of slope of the composition profile; this is illustrated in 3(b).

Figure 4 Composition profiles of $^{185}Re^{+3}$ (61.6 to 61.9 amu) and $^{187}Re^{+3}$ (62.3 to 62.6 amu) in a W-25 at.% Re alloy. The average composition obtained from these plots are 10.6 at.% $^{185}Re$ and 14.8 at.% $^{187}Re$ for a total Re concentration of 25.4 at.% as determined from the average slopes. A least squares fit to the (m/n) histogram which takes into account the overlapping tails caused by energy deficits yields an average Re composition of 22 ± 2 at.% which agrees with the nominal composition.

Figure 5 The Ti spectrum from a Mo-1.0 at.% Ti alloy. The five stable Ti isotopes are clearly visible and their isotopic abundances agree with the expected values as shown in Table 1.

Figure 6 Semilogarithmic plot of the (m/n) spectrum for TZM. Note that the seven isotopes of Mo, the $^{90}Zr$ isotope and four of the five isotopes of Ti are clearly visible. The absence of $^{46}Ti$ and $^{91}Zr$ peaks are not surprising since these isotopes

would be expected to produce only 1±1 event on a statistical basis. The Ti concentration corresponds to 0.26 at.% Ti and the Zr concentration corresponds to 0.13 at.% Zr. Note the total absence of background counts resulting from the low background pressure ($4.5 \cdot 10^{-10}$ Torr).

Figure 7 Composition profiles for Ti and Zr in TZM. The Ti appears to be uniformly distributed in the material whereas the Zr is concentrated in a single cluster.

Figure 8 Semilogarithmic plot of the (m/n) spectrum of LS1A. The main constituents (Fe, Ni and Cr) as well as the minor alloying additions with concentrations of fractions of an atomic percent (Mn, Mo, Si and Ti) are easily detected by the atom probe technique. The average compositions determined from this histogram are listed in Table 2.

Figure 9 Semilogarithmic plot of the (m/n) spectrum for Metglas 2826. The average concentration of Fe, Ni, P and B in this metallic glass are easily measured by the atom probe technique and are given in Section 5. Note the random background counts which are clearly visible in this semilogarithmis plot caused by the $1 \cdot 10^{-7}$ Torr Ne imaging gas present during the atom probe analysis. Compare this with figure 6 for TZM which was recorded at a pressure of $4.5 \cdot 10^{-10}$ Torr and which shows no background counts.

Figure 10 The composition profiles for boron and phosphorus in Metglas 2826; this specimen was heated to 420 K for less than 6 h.

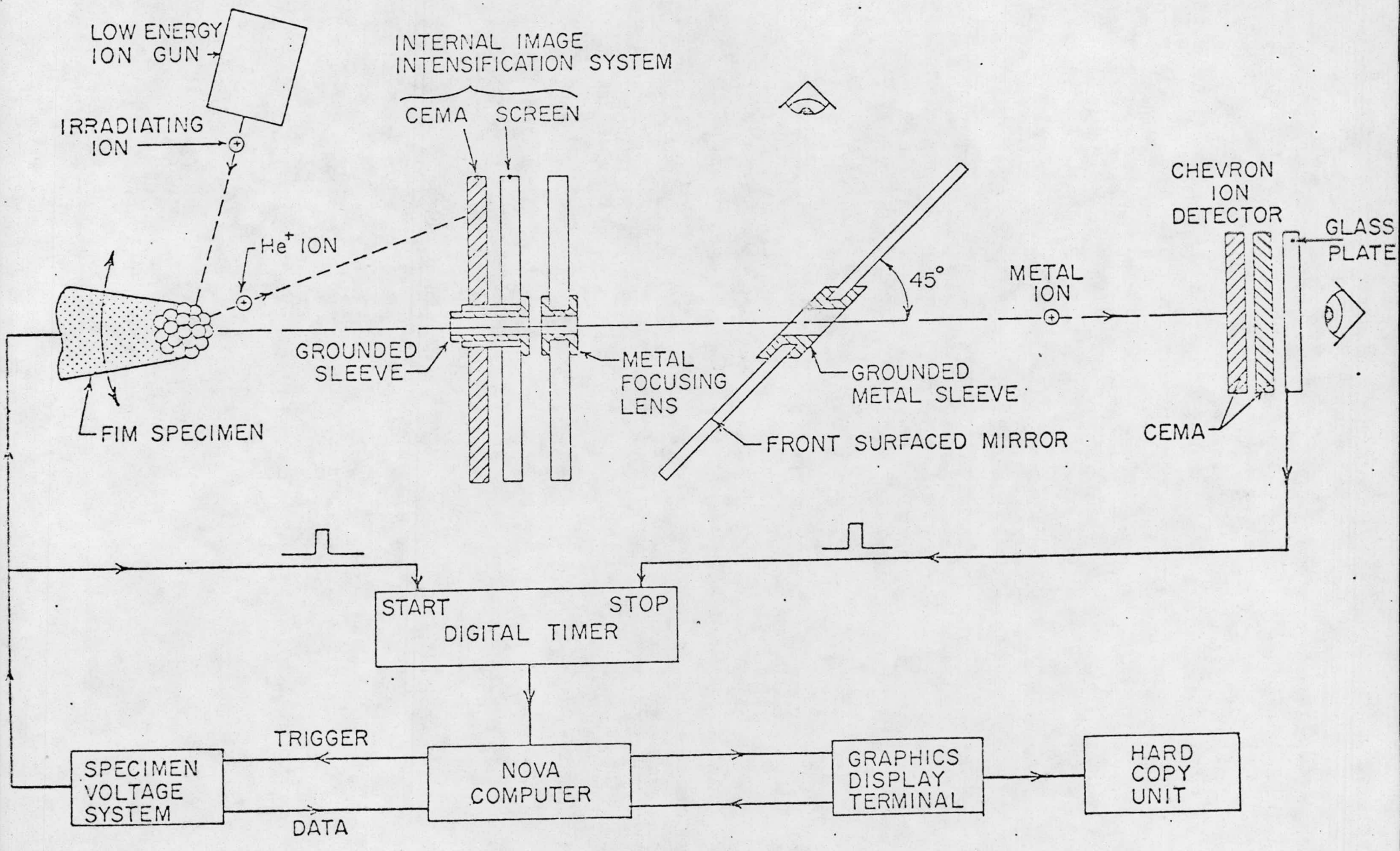
LOW ENERGY ION GUN
IRRADIATING ION
INTERNAL IMAGE INTENSIFICATION SYSTEM
CEMA
SCREEN
He+ ION
CHEVRON ION DETECTOR
GLASS PLATE
45°
METAL ION
GROUNDED SLEEVE
METAL FOCUSING LENS
GROUNDED METAL SLEEVE
FIM SPECIMEN
FRONT SURFACED MIRROR
CEMA
START
STOP
DIGITAL TIMER
TRIGGER
SPECIMEN VOLTAGE SYSTEM
NOVA COMPUTER
GRAPHICS DISPLAY TERMINAL
HARD COPY UNIT
DATA

Fig. 1

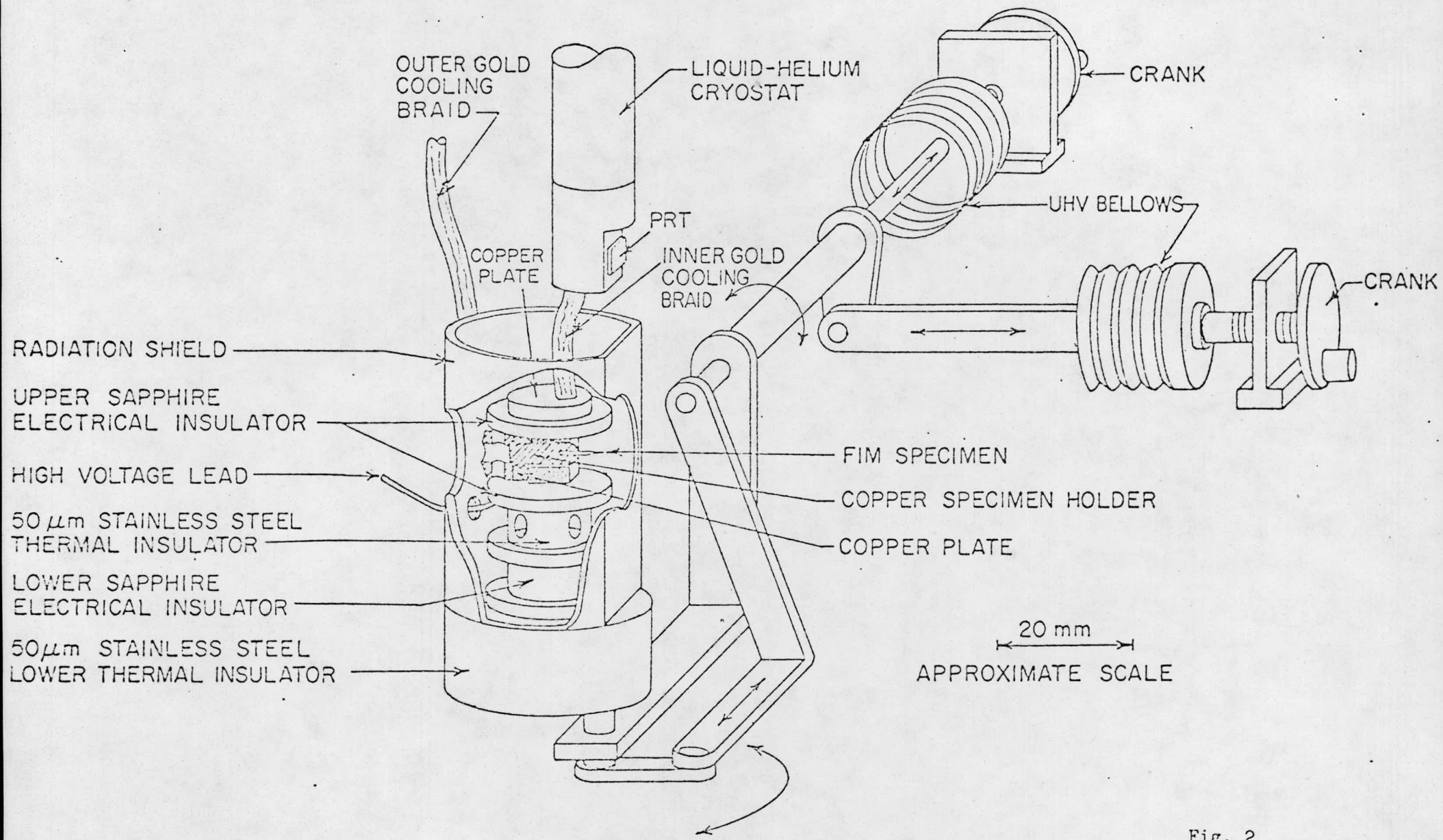
OUTER GOLD COOLING BRAID
LIQUID-HELIUM CRYOSTAT
CRANK
UHV BELLOWS
PRT
COPPER PLATE
INNER GOLD COOLING BRAID
CRANK
RADIATION SHIELD
UPPER SAPPHIRE ELECTRICAL INSULATOR
HIGH VOLTAGE LEAD
50 μm STAINLESS STEEL THERMAL INSULATOR
LOWER SAPPHIRE ELECTRICAL INSULATOR
50μm STAINLESS STEEL LOWER THERMAL INSULATOR
FIM SPECIMEN
COPPER SPECIMEN HOLDER
COPPER PLATE
20 mm
APPROXIMATE SCALE

Fig. 2

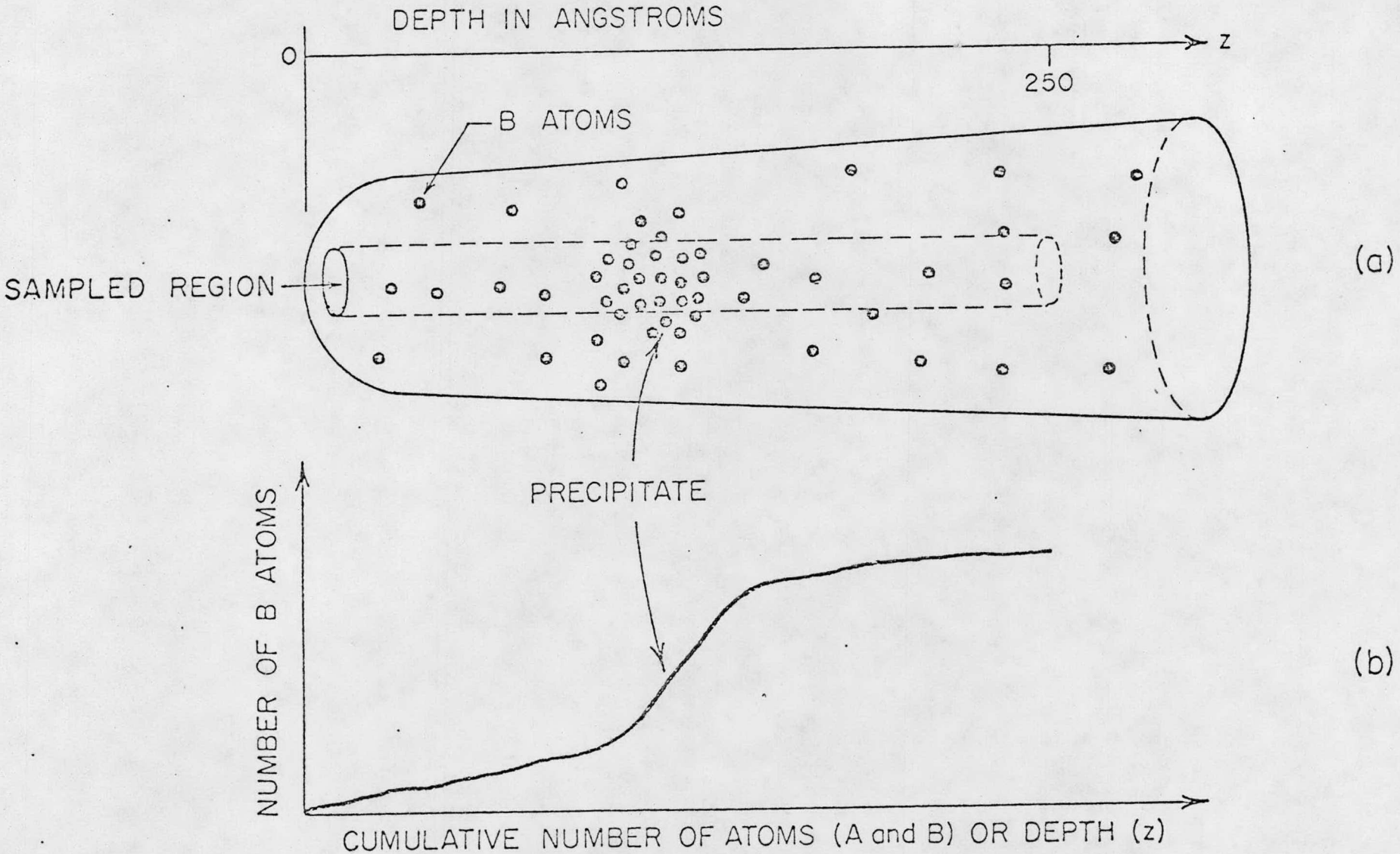
DEPTH IN ANGSTROMS
0
z
250
B ATOMS
SAMPLED REGION
(a)
PRECIPITATE
NUMBER OF B ATOMS
(b)
CUMULATIVE NUMBER OF ATOMS (A and B) OR DEPTH (z)

Fig. 3

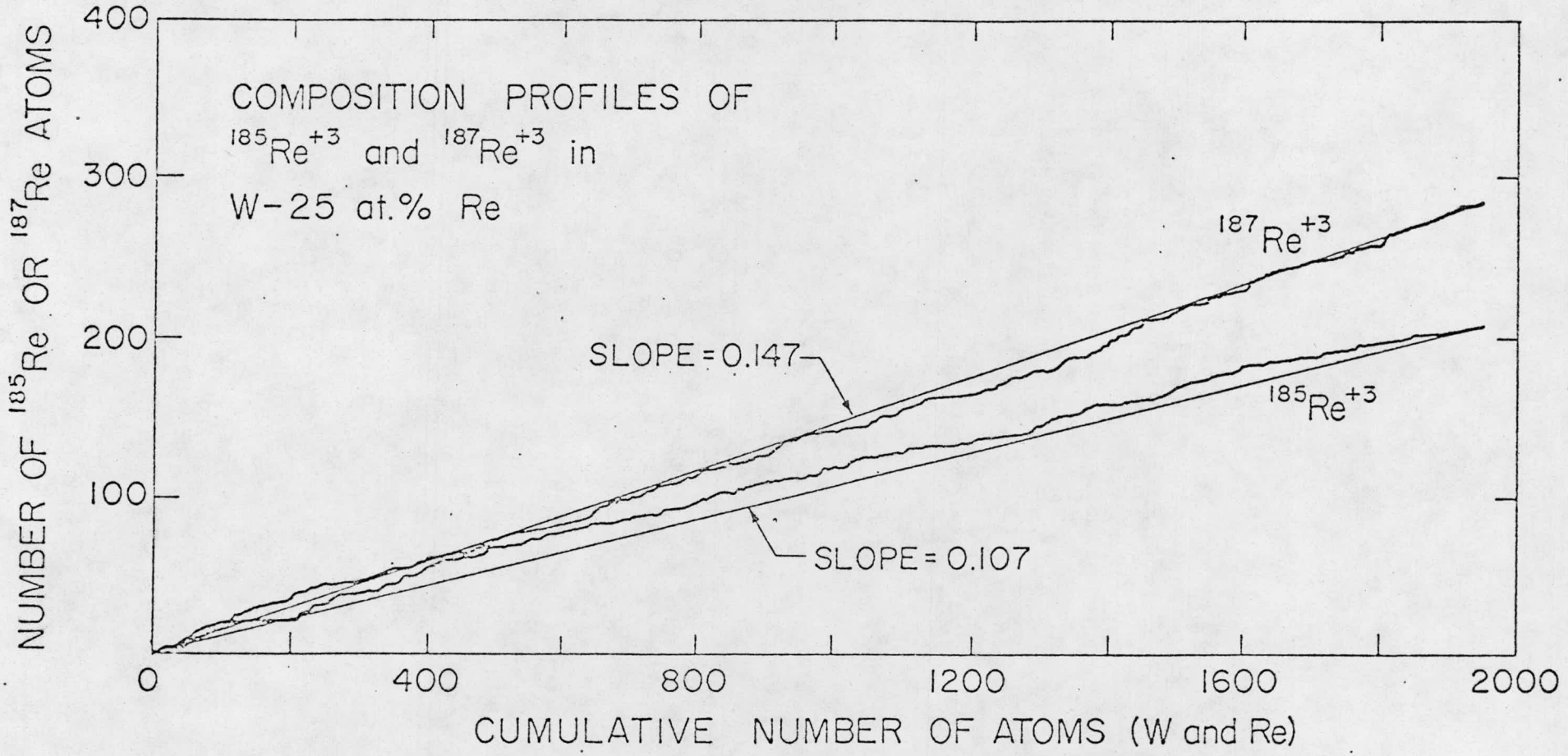
COMPOSITION PROFILES OF
$^{185}Re^{+3}$ and $^{187}Re^{+3}$ in
W-25 at.% Re
$^{187}Re^{+3}$
$^{185}Re^{+3}$
SLOPE = 0.147
SLOPE = 0.107
NUMBER OF $^{185}Re$ OR $^{187}Re$ ATOMS
CUMULATIVE NUMBER OF ATOMS (W and Re)
0
400
800
1200
1600
2000
100
200
300
400

Fig. 4

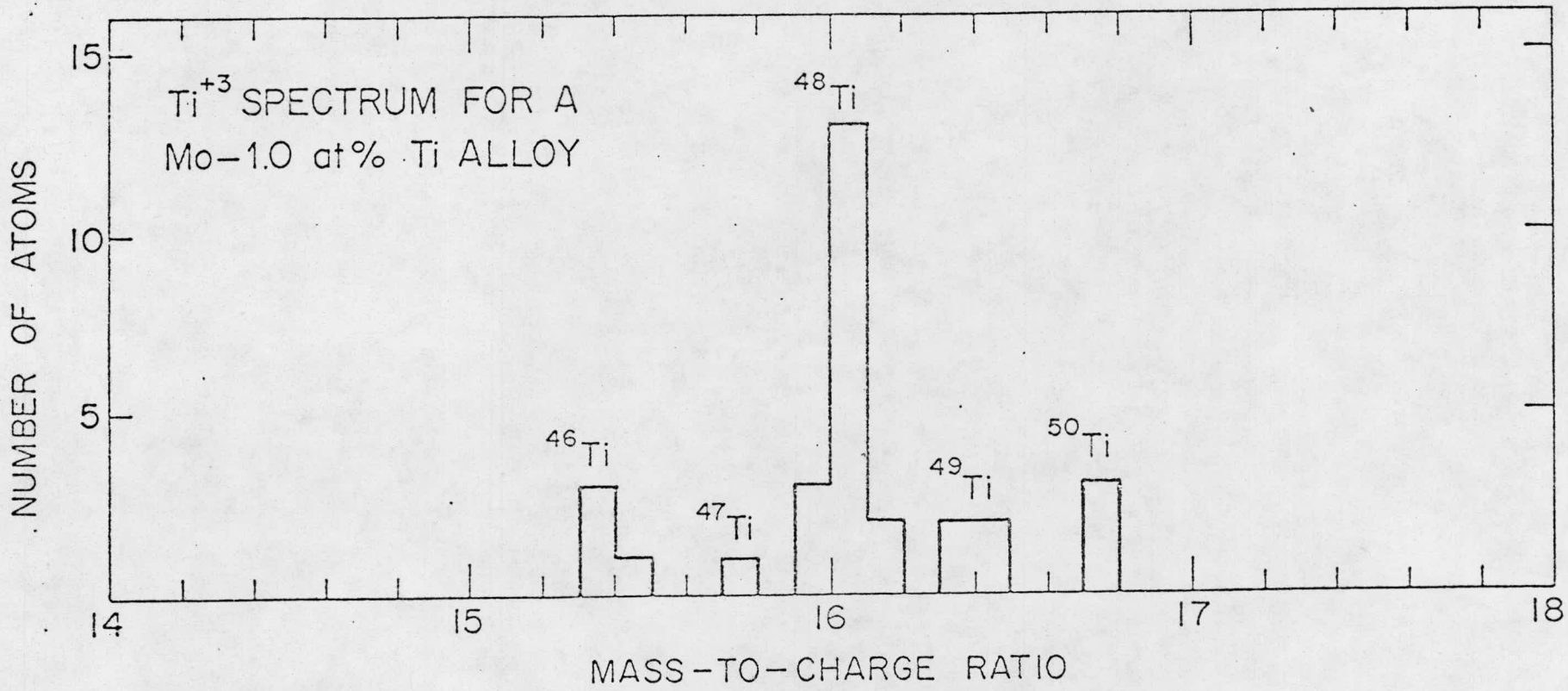
Ti+3 SPECTRUM FOR A
Mo–1.0 at% Ti ALLOY
48Ti
46Ti
47Ti
49Ti
50Ti
NUMBER OF ATOMS
15
10
5
14
15
16
17
18
MASS-TO-CHARGE RATIO

Fig. 5

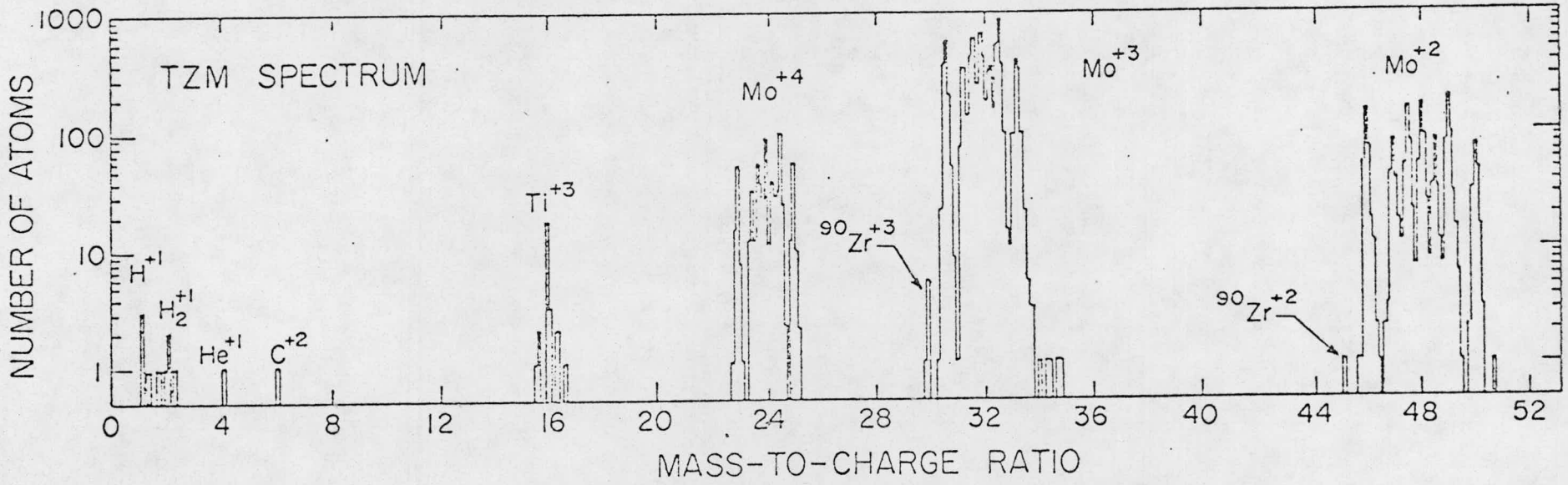
TZM SPECTRUM
NUMBER OF ATOMS
1000
100
10
1
H+1
H2+1
He+1
C+2
Ti+3
Mo+4
90Zr+3
Mo+3
90Zr+2
Mo+2
0
4
8
12
16
20
24
28
32
36
40
44
48
52
MASS-TO-CHARGE RATIO

Fig. 6

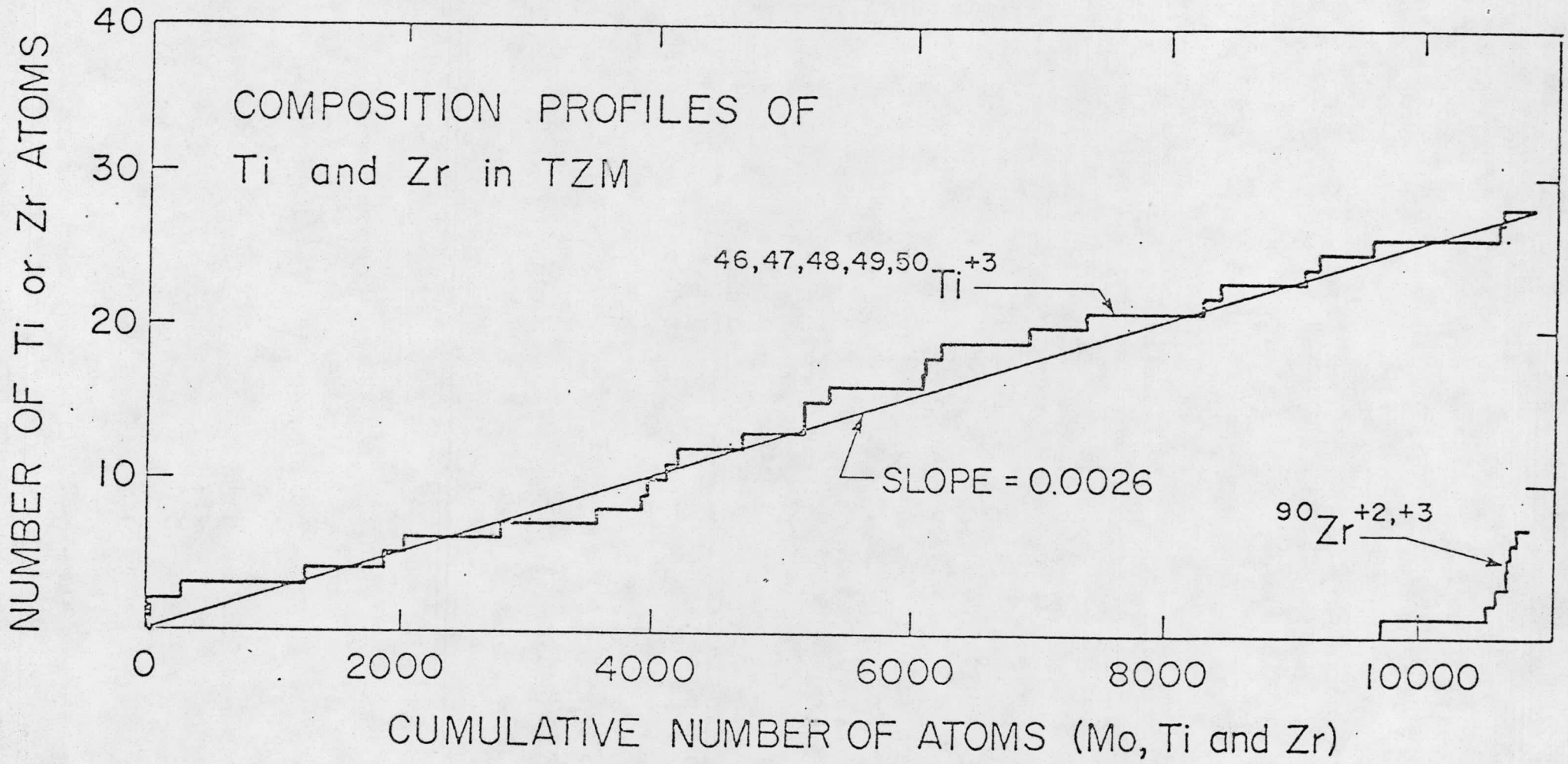
COMPOSITION PROFILES OF
Ti and Zr in TZM
46,47,48,49,50 Ti +3
SLOPE = 0.0026
90 Zr +2,+3
NUMBER OF Ti or Zr ATOMS
CUMULATIVE NUMBER OF ATOMS (Mo, Ti and Zr)
0
2000
4000
6000
8000
10000
10
20
30
40

Fig. 7

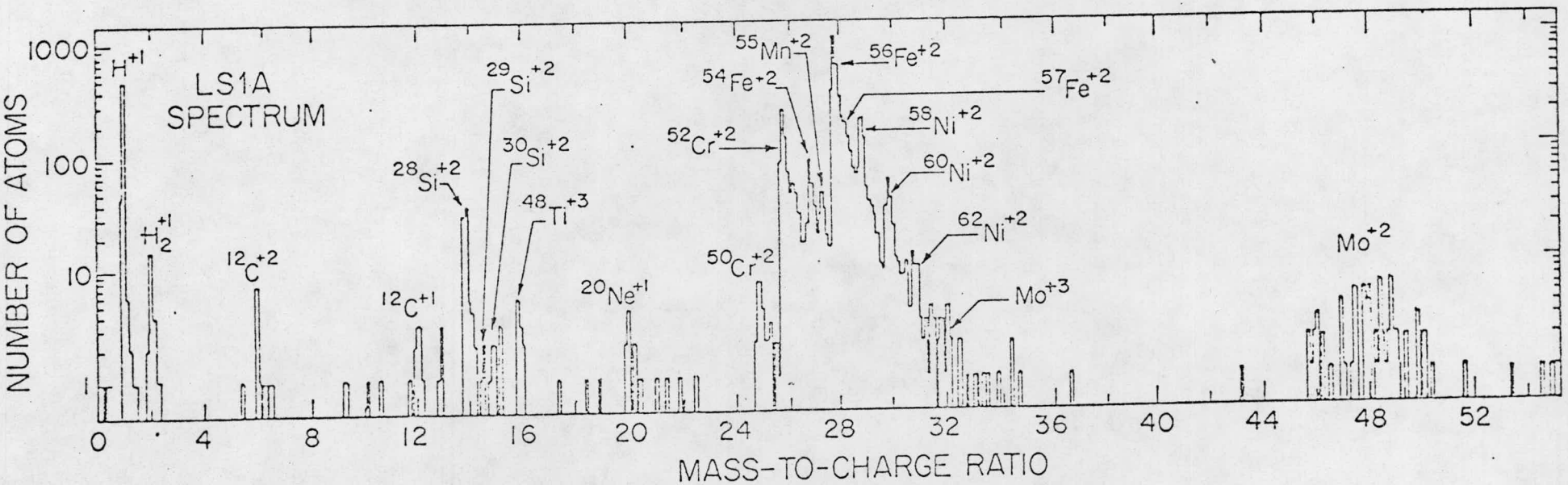
LS1A
SPECTRUM
NUMBER OF ATOMS
MASS-TO-CHARGE RATIO
1000
100
10
1
0
4
8
12
16
20
24
28
32
36
40
44
48
52
H+1
H2+1
12C+2
12C+1
28Si+2
29Si+2
30Si+2
48Ti+3
20Ne+1
50Cr+2
52Cr+2
54Fe+2
55Mn+2
56Fe+2
57Fe+2
58Ni+2
60Ni+2
62Ni+2
Mo+3
Mo+2

Fig. 8

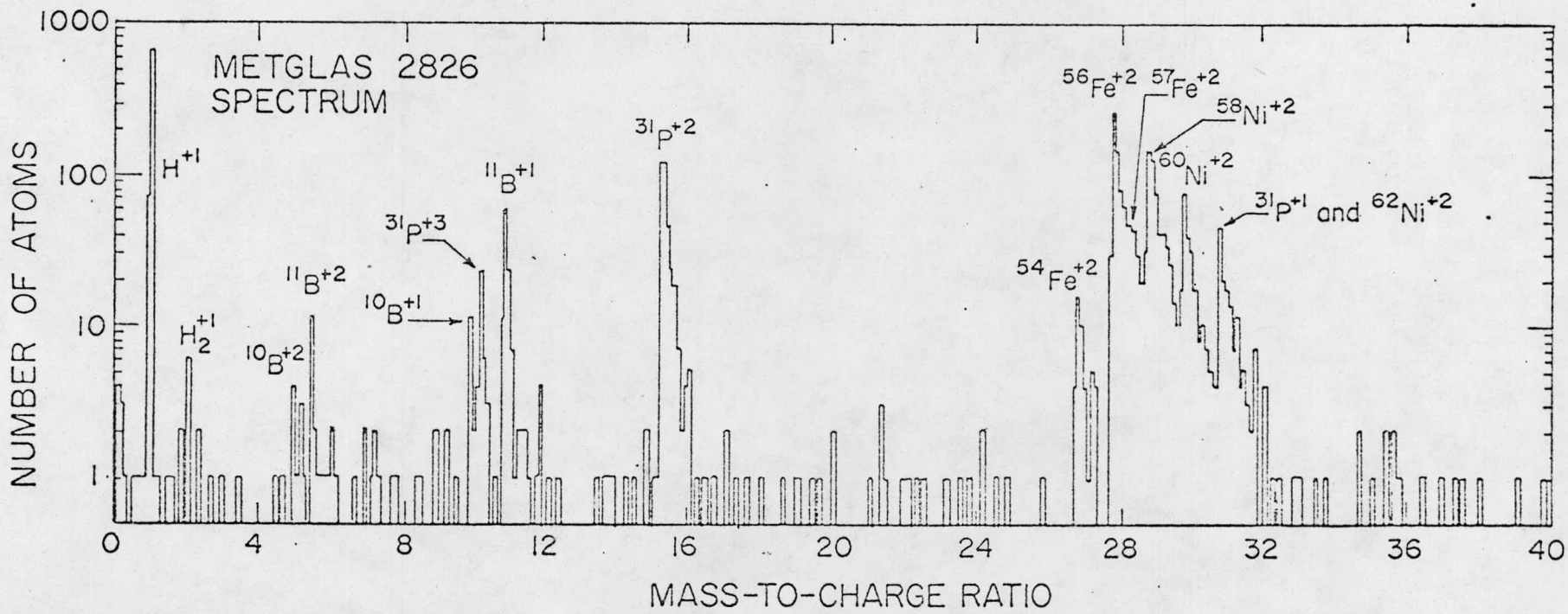
METGLAS 2826
SPECTRUM
NUMBER OF ATOMS
MASS-TO-CHARGE RATIO
1000
100
10
1
0
4
8
12
16
20
24
28
32
36
40
H+1
H2+1
10B+2
11B+2
10B+1
31P+3
11B+1
31P+2
54Fe+2
56Fe+2
57Fe+2
58Ni+2
60Ni+2
31P+1 and 62Ni+2

Fig. 9

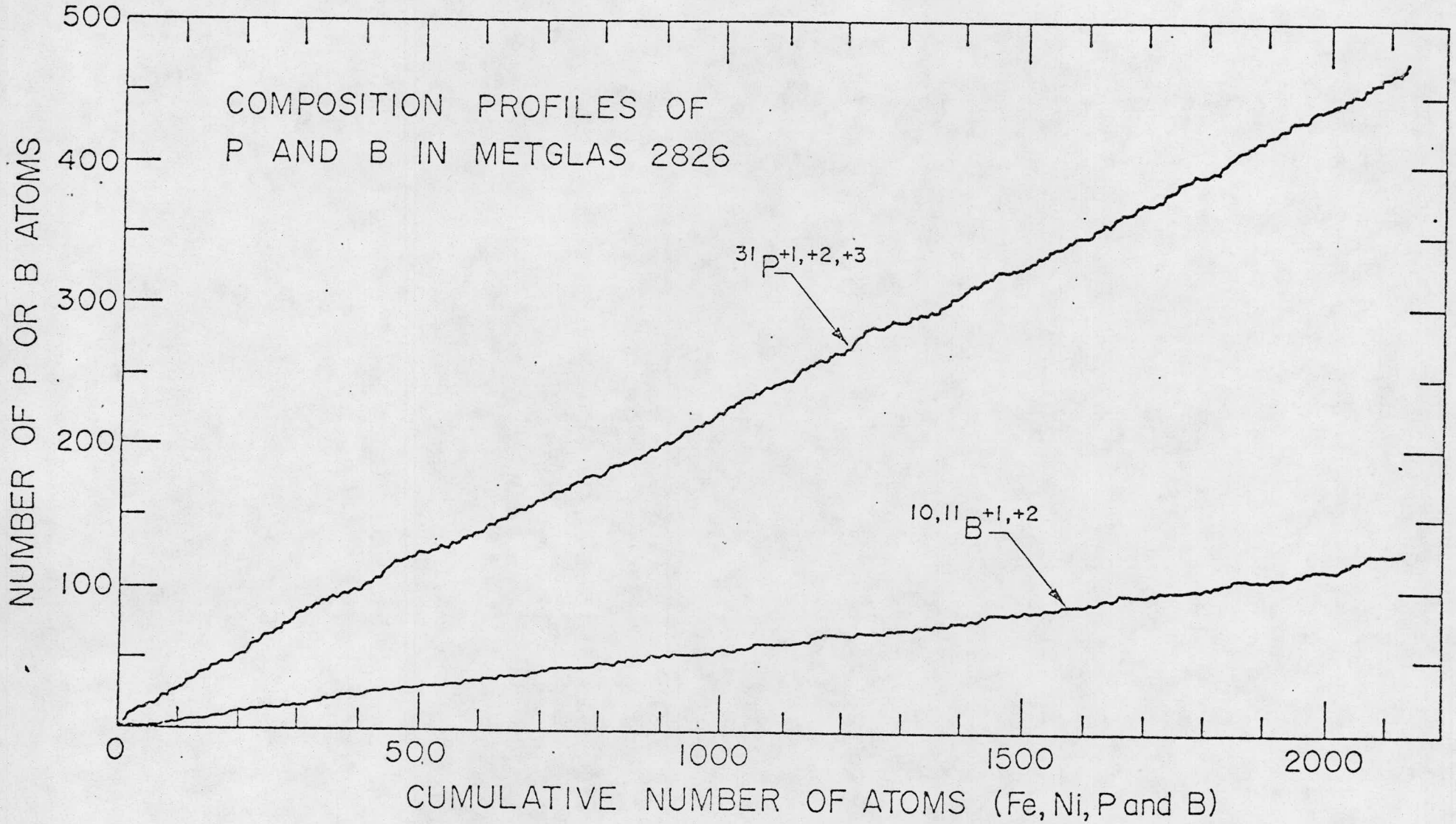
COMPOSITION PROFILES OF
P AND B IN METGLAS 2826
31 P+1,+2,+3
10,11 B+1,+2
NUMBER OF P OR B ATOMS
CUMULATIVE NUMBER OF ATOMS (Fe, Ni, P and B)
0
500
1000
1500
2000
100
200
300
400
500

Fig. 10